



Revealing hetero-deformation induced (HDI) stress strengthening effect in laminated Al-(TiB₂+TiC)_p/6063 composites prepared by accumulative roll bonding

Yuyao Chen^a, Jinfeng Nie^{a,*}, Fang Wang^a, Huabing Yang^b, Chongchong Wu^b,
Xiangfa Liu^b, Yonghao Zhao^{a,**}

^a Nano and Heterogeneous Materials Center, Nanjing University of Science and Technology, Nanjing, 210094, China

^b Key Laboratory for Liquid-Solid Structural Evolution and Processing of Materials, Ministry of Education, Shandong University, Jinan, 250061, China



ARTICLE INFO

Article history:

Received 30 July 2019

Received in revised form

12 September 2019

Accepted 13 September 2019

Available online 14 September 2019

Keywords:

Aluminum alloys

Laminated composites

Accumulative roll bonding (ARB)

Mechanical properties

HDI hardening

ABSTRACT

Laminated metal composites as a type of heterostructured materials, consisting of two or more metals, have attracted extensive attention for their excellent mechanical properties, electrochemistry characteristics and corrosion resistance. In this study, an Al-(TiB₂+TiC)_p/6063 laminated composite was successfully prepared for the first time using accumulative roll bonding (ARB) process up to three cycles. The particle distribution in Al-(TiB₂+TiC)_p layer became more dispersive with the increasing ARB cycles and the matrix α -Al grains were also refined significantly. The interfaces of 6063 and Al-(TiB₂+TiC)_p layers were well bonded and kept straight without any necking or fracture during the plastic deformation. The tensile strength and ductility of the laminated composites were increased simultaneously with increasing ARB cycles. Ultimate tensile strength, yield stress and elongation to failure of the composites increase to 255.8 MPa, 247.4 MPa and 11.6% after three ARB cycles, increased by 21.9%, 22.4% and 17.2%, respectively. It is revealed that hetero-deformation induced (HDI) stress played a crucial role in significant enhancement of tensile strength and ductility for the laminated composites.

© 2019 Elsevier B.V. All rights reserved.

1. Introduction

With the development of modern technology, single material hardly satisfies the increasing demands of properties. Laminated metal composites (LMCs), consisting of two or more metals, have been developed for their excellent mechanical properties, electrochemistry characteristics and corrosion resistance [1–3]. Actually, LMCs as a type of heterostructured (HS) materials have recently attracted extensive attention from the materials community [4]. During tensile deformation of HS materials, the soft domains will start plastic deformation first while the hard domains remain elastic. In this elastic-plastic deformation stage, geometrically necessary dislocations (GNDs) will be blocked by and pile up against domain boundaries, which produces long-range internal stress, i.e. back stress, in the soft domain. Back stress is believed to make the heterostructured materials stronger [5]. At the

fundamental level, the heterostructure leads to hetero-deformation among HS domains [6]. Then the hetero-deformation leads to the development of back stress and forward stress, which collectively produces the strengthening and extra work hardening, which is described more accurately as the hetero-deformation induced (HDI) hardening in the latest literature [4].

However, the vast majority of research work focus on the metal-metal laminated composites, such as Al/Al, Al/Fe and Cu/Zn [7–9]. Recently, particle-reinforced aluminum matrix composites (PRAMCs) have received increasing attention due to their high specific strength, high stiffness and good wear resistance [10–12]. While their low ductility limits their wide applications. In order to further improve the comprehensive mechanical properties of the Al matrix composites, the particles distributions and their architectures were tailored by following deformation process, such as rolling, extrusion, accumulative roll-bonding (ARB) and high pressure torsion (HPT) [13–16]. ARB process is considered to be the most promising severe plastic deformation process (SPD) in practical industry, since it does not require any major modification of equipment design as well as production in continuous form is

* Corresponding author.

** Corresponding author.

E-mail address: niejinfeng@njust.edu.cn (J. Nie).

feasible [17–19]. M. Alizadeh et al. [20] fabricated the nano-structured Al–SiC_p composites by accumulative roll bonding (ARB) process, leading to a uniform distribution of the reinforcement particles and a distinct increase in strength.

In the present work, an Al-(TiB₂+TiC)_p composite was selected as one of laminated component, and the laminated structure were designed to improve the mechanical properties. The laminated composites were fabricated by accumulative rolling of alternately stacked Al-(TiB₂+TiC)_p composite sheets and 6063 sheets.

The microstructure and mechanical properties of the Al-(TiB₂+TiC)_p/6063 laminated composites with different ARB cycles were investigated. Especially, HDI stress strengthening in laminated Al-(TiB₂+TiC)_p/6063 composites was evaluated.

2. Experimental

2.1. Fabrication of the laminated composites

The raw materials used in this study are 6063Al alloy and Al-5(TiB₂+TiC) (Al-3.6TiB₂-1.4TiC) composites prepared by in-situ synthesis (as mentioned in our previous work [15]). The chemical compositions (all compositions quoted in this work are in wt.% unless otherwise stated) of 6063Al alloy are shown in Table 1.

The 6063 alloy and Al-(TiB₂+TiC)_p specimens with dimensions of 50 × 26 × 2 mm³ were machined for ARB processes. Firstly, the 6063 sheets were treated at 530 °C for 2 h in a resistance furnace and then quenched in cold water, and then the 6063 and Al-(TiB₂+TiC)_p sheets were subjected to the ARB process. A schematic illustration of the ARB process is shown in Fig. 1. The contact surface was degreased and decontaminated by acetone and wire brushing to provide rough surfaces and then stack the sheets together and fix the four corners with wire to achieve a good bonding between sheets. The stacked sheets were preheated for 10 min at 530 °C in a resistance furnace and then rolled for 50% reduction in thickness without using lubricant. Then the roll-bonded composite sheet was cut in half and stacked to the initial thickness. The stacked sheets were again preheated at 530 °C and rolled with the same reduction ratio, and then the same procedure was repeated up to three cycles. Finally, the obtained laminated composites were put into oil bath furnace for 2 h at 175 °C for aging treatment.

2.2. Microstructure characterization and tensile tests

The microstructures of the ARB processed specimens were characterized using a field emission scanning electron microscope (FESEM, Quanta 250 F, FEI, Hillsboro, OR, USA) equipped with an energy dispersive spectroscopy (EDS, Oxford Instruments, Oxford, UK), X-ray diffraction (XRD, D8, Bruker, Coventry, Germany) and Electron back-scattered diffraction (EBSD) test. Specimens for SEM/EBSD characterization were prepared by mechanical polishing. The operation voltage for SEM and EBSD scanning were 20 kV and 15 kV, respectively, and the step size for EBSD scanning was 0.15 μm. Due to the limitation of angular precision, misorientation below 2° were not measured in order to avoid spurious boundaries. EBSD data were analyzed using the Channel 5 software. And all the microstructures were observed on the rolling direction-normal direction (RD-ND) plane of the sheets. A Vickers microhardness experiment was conducted on the surface of rolling direction-

transverse direction (RD-TD) plane of the multilayered composites using a tester (HMV-G 21DT, Shimadzu, Tokyo, Japan) at a load of 0.49 N held for 15 s. For each specimen, at least ten randomly selected points were tested to obtain a mean value with a standard deviation error.

The tensile test specimens were machined from the processed sheets with a gauge size of 15 × 2.5 × 2 mm³ oriented along the rolling direction (RD) in accordance with the ASTM: E8M standard. The tensile direction of the specimen was also parallel to the RD of the sheets and tensile samples were tested at room temperature with a universal tensile testing machine (LFM-20, Walter + baig, Löhningen, Switzerland) at an initial strain rate of 5.6 × 10⁻⁴ s⁻¹.

3. Results and discussions

3.1. Microstructure of the laminated composites

Fig. 2 shows the microstructure of Al-(TiB₂+TiC)_p/6063 composites on RD-ND planes under different ARB cycles. The interfaces between 6063 and Al-(TiB₂+TiC)_p layers formed during each cycle were straight and no obvious cracks were observed (Fig. 2a–c), indicating that deformation of the two layers during rolling process seemed to be almost homogenous and a good bonding between layers was achieved. Both the average layer thickness of 6063 and Al-(TiB₂+TiC)_p are similar and was reduced from about 2 mm to 240 μm after three cycles. Generally, the compatible co-deformation is determined by the elastic modulus and flow properties of each layer [21,22]. Therefore, it is considered that the similar flow behavior of 6063 and Al-(TiB₂+TiC)_p layers leads to the good atomic bonding at the interfaces during the ARB treatment [23].

Fig. 3 shows EDS line-scanning analysis of the interfaces of Al-(TiB₂+TiC)_p/6063 laminated composites after three cycles. As shown in Fig. 3b, the high peak of Ti element arises from TiC and TiB₂ particles. While, it is noted that a Mg element distribution gradient was formed at the interface, indicating that Mg diffused into the adjacent Al-(TiB₂+TiC)_p composite layer during the treatment. As a result, the diffusion of alloying elements at the interfaces promoted the good atomic bonding at interfaces.

The particle distribution in Al-(TiB₂+TiC)_p layer was shown in Fig. 4. It indicates that TiB₂ and TiC reinforcement particles were uniformly distributed in the Al matrix after the treatment and its distribution became more uniform along the RD direction with increasing ARB cycles (Fig. 4a–c). The morphology of the particles can be clearly observed at a higher magnification shown by SEM (Fig. 4d–f) and the mean size is about 2 μm.

In order to evaluate the grain structure of the aluminum matrix during the deformation, EBSD maps of these samples on the RD-ND planes were shown in Fig. 5. As shown in Fig. 5a, as-cast structure consists of equiaxed grains with an average size of ~35.2 μm. While, α-Al grains are elongated along RD direction during the ARB treatment as shown in Fig. 5b and c. The mean grain size was reduced to ~15.5 μm after one cycle. As the rolling cycle increases, the average grain size decreased continually to ~8.9 μm and 6.5 μm after two and three cycles, respectively. Especially, after two cycles, many small grains can be observed in Fig. 5c and d, indicating a significant grain refinement has been achieved at a higher deformation strain.

Fig. 6 shows the misorientation angle distribution of Al-(TiB₂+TiC) layer after different ARB cycles. It shows that mean misorientation angle is increased from 13° to 19°, and the fraction of high angle grain boundaries (misorientation angle larger than 15°, HAGBs) reaches up to ~26% after one cycle. With increasing strain, these values increase to ~15° and 34% after two cycles, respectively. The high fraction of LAGBs indicates that a large

Table 1
Chemical compositions of the 6063 and the Al-(TiB₂+TiC)_p (wt.%).

Alloy	Mg	Si	Fe	Cu	Al
6063	0.64	0.63	0.11	0.03	Bal.

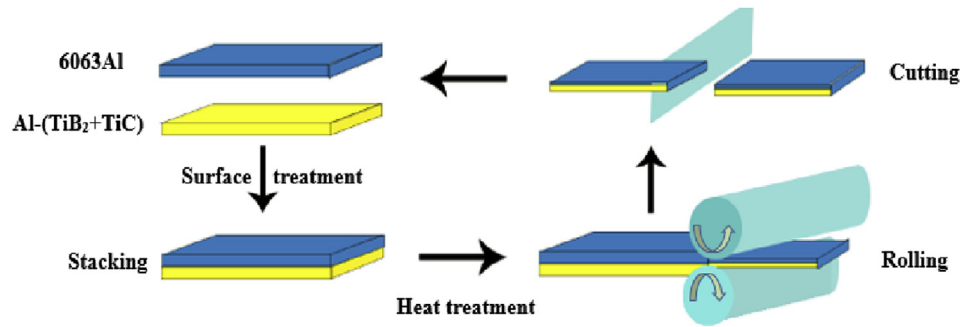


Fig. 1. Diagrammatic illustration of the accumulative roll-bonding (ARB) process.

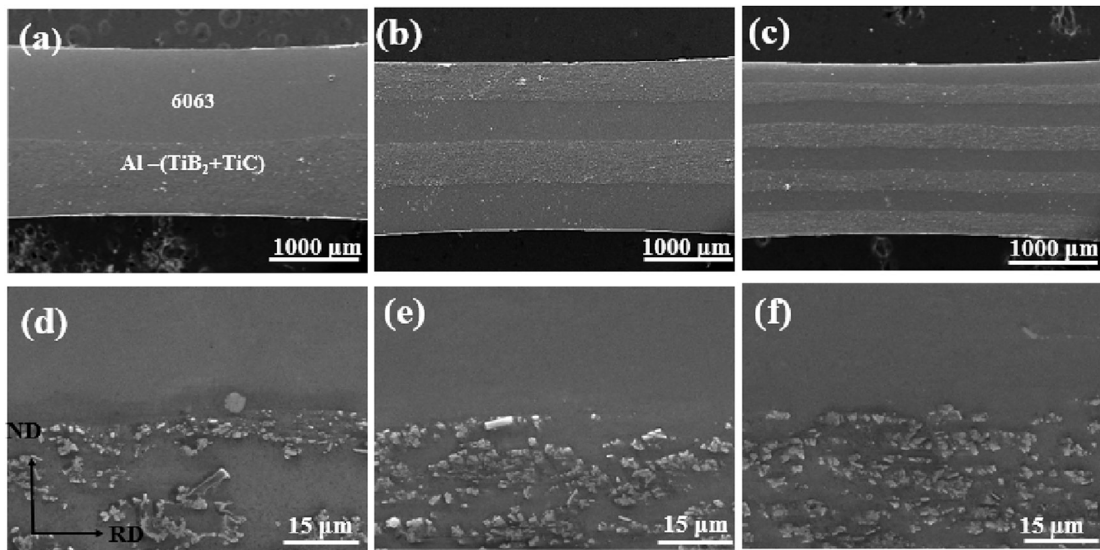


Fig. 2. SEM micrographs of the Al-(TiB₂+TiC)/6063 composites after (a, d) one; (b, e) two; (c, f) three cycles.

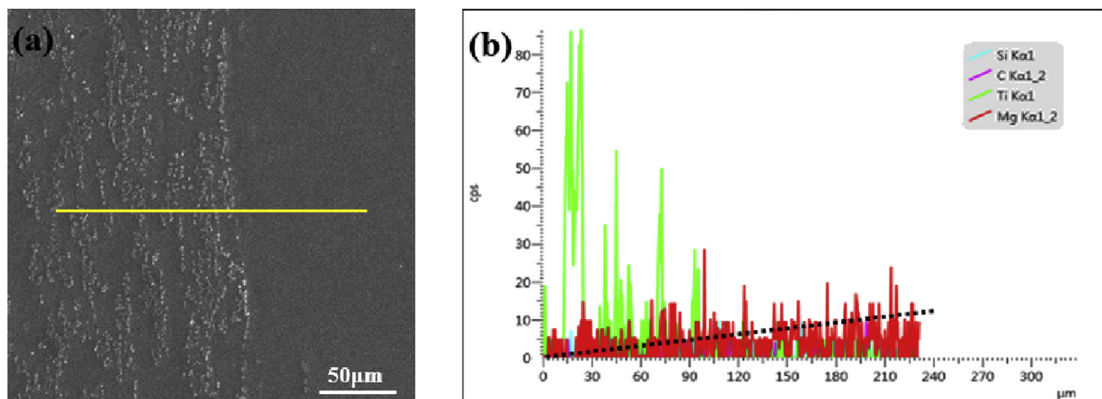


Fig. 3. SEM micrograph and the EDS analysis of the Al-(TiB₂+TiC)_p/6063 composite.

number of sub-boundaries were formed by the dislocation tangles during the ARB deformation and the elongated grains were mainly composed of sub-grains. While, with the increase of deformation strain, sub-grain boundaries turn into high angle grain boundaries and then the fraction of HAGBs increase to about 43% after three cycles. Also, the mean misorientation angle of the boundaries increased and the grain size decreased. Finally, a typical rolling structure containing large amount of coarse elongated grains along

RD and some fine grains was obtained. Based on the conventional dislocation theory, a very high dislocation density is created at the primary stage of deformation, which leads to the formation of an intragranular cell structures with thick cell walls and low angles of misorientation. These walls convert to grain boundaries, and finally arrays of ultra-fine grains with HAGBs are formed.

The interface grain structures of 6063/Al-(TiC + TiB₂)_p laminated composite after different ARB cycles are shown by EBSD

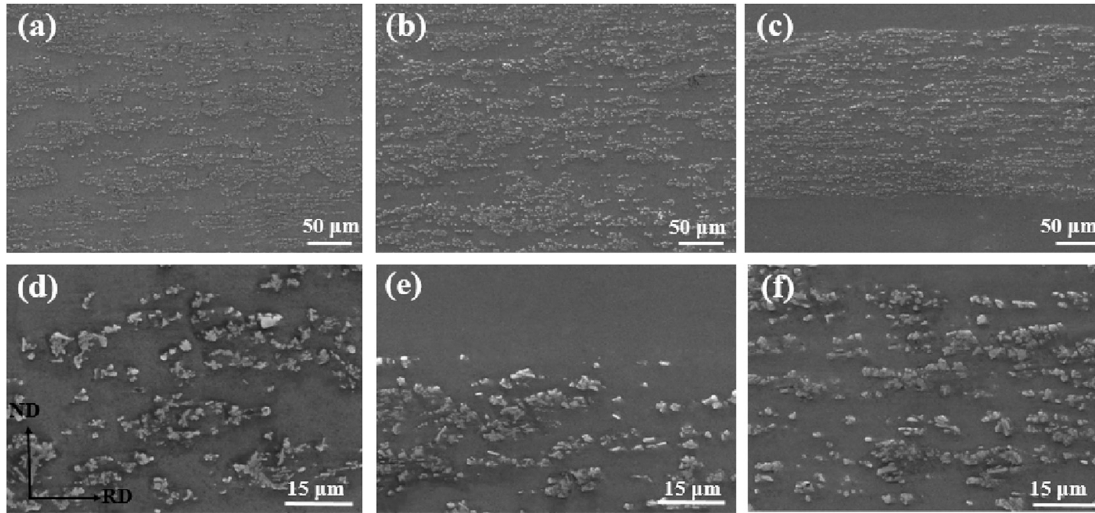


Fig. 4. Particle distributions in Al-(TiB₂+TiC) layer after (a, d) one; (b, e) two; (c, f) three cycles.

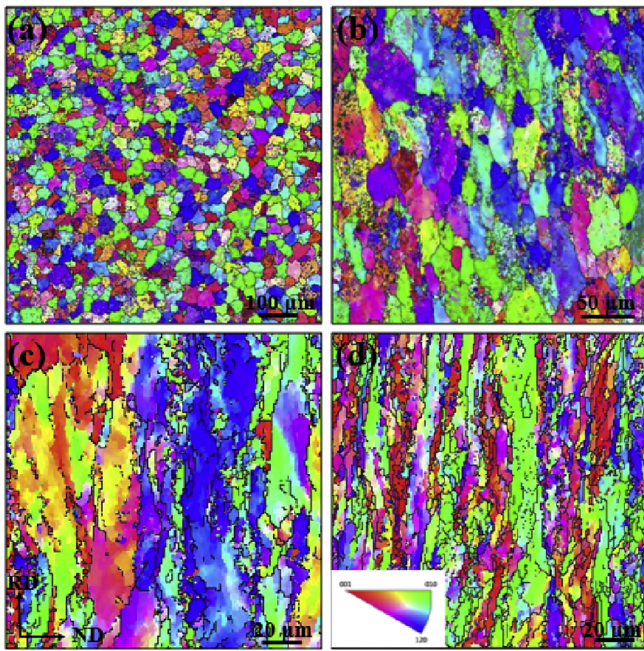


Fig. 5. EBSD maps of Al-(TiB₂+TiC)_p layer in the laminated composites before and after ARB treatments: (a) as-cast; (b) one; (c) two; (d) three cycles.

maps (Fig. 7a–c), respectively. It can be seen that the two layers are well bonded without any obvious cavities or cracks. Meanwhile, an obvious grain size difference existed between the two layers, which can be considered as a bimodal structure; the coarse grains in the 6063 layer reach up to 120 μm, while the fine grains in the Al-(TiC + TiB₂) layer was below than 6.5 μm as shown in Fig. 7a. With the increase of ARB cycles, α-Al grains in both layers are elongated along RD (Fig. 7b and c). In Fig. 7a–c, the white circles indicate the matrix grains at the interface with a width of about 10–20 μm, which shows that the grains were significantly refined. It is considered that the high shearing stress at the interfaces during rolling deformation promotes the dynamic recrystallization in the local area.

3.2. Tensile mechanical properties of the laminated composites

The engineering stress-strain curves of the laminated composites after different cycles and the following aging treatment are illustrated in Fig. 8a and the detail is given in Table 2. It shows that both the ultimate tensile strength (UTS) and yield strength (YS) of the laminated composite have been enhanced significantly to ~209.8 MPa and 202.1 MPa after the first ARB cycle, while maintaining a reasonable ductility of ~9.9%. UTS of the composite after the first cycle is improved by ~37.9% and 15.6%, compared with that of original Al-(TiC + TiB₂)_p and 6063. According to role of mixture:

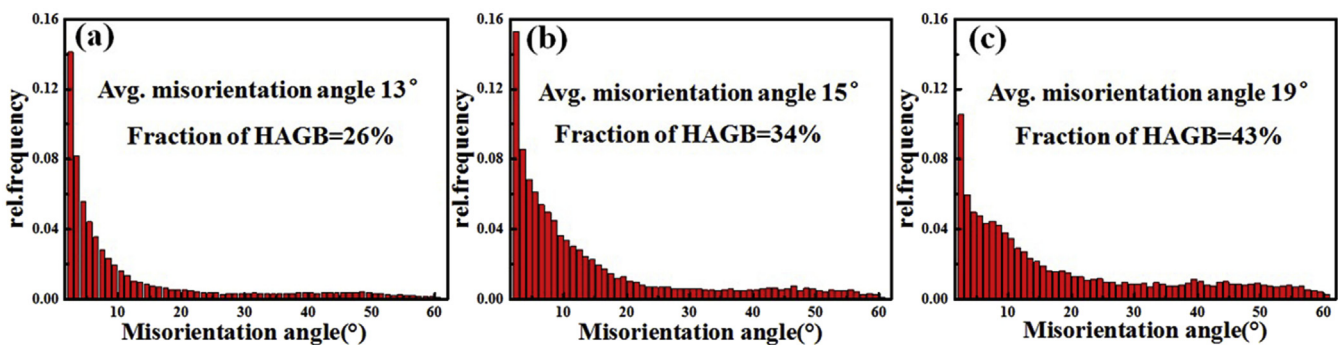


Fig. 6. The misorientation angle distribution of Al-(TiB₂+TiC) processed by ARB after different cycles: (a) one; (b) two; (c) three cycles.

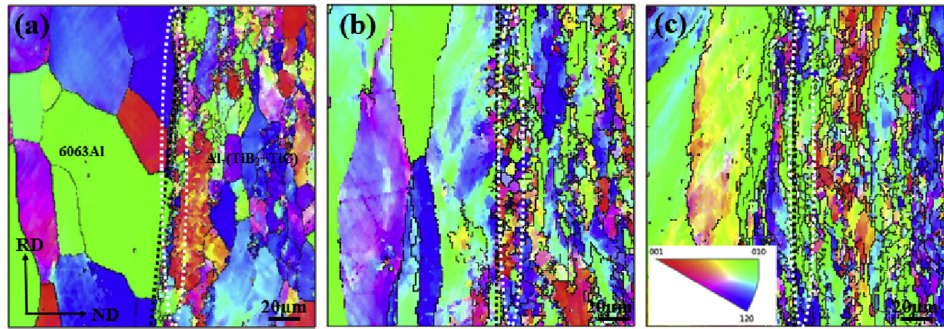


Fig. 7. EBSD maps of interfaces of the laminated composites after different ARB cycles: (a) one; (b) two; (c) three cycles.

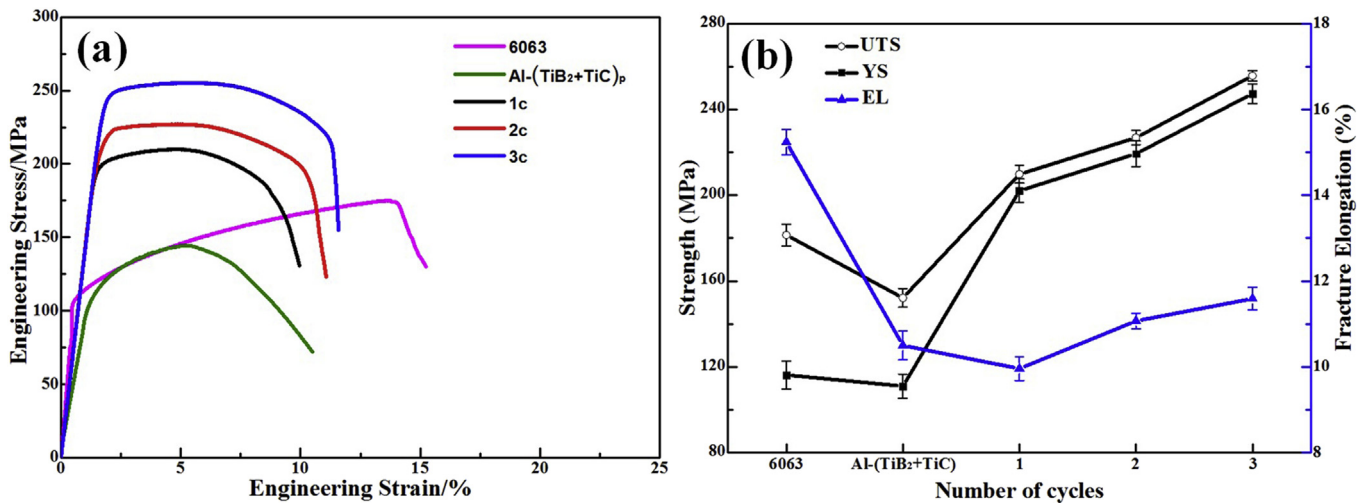


Fig. 8. (a) Engineering stress-strain curves of the Al-(TiB₂+TiC)_p/6063 composites with different cycles; (b) UTS, YS and EL variations of the composites for various cycles.

Table 2
Mechanical properties of the laminated composites with different cycles.

Sample	UTS/MPa	YS/MPa	EL/%
1c	209.8	202.1	9.9
2c	226.9	219.4	11.1
3c	255.8	247.4	11.6
6063	181.5	116.3	15.2
Al-(TiB ₂ +TiC) _p	152.1	111.2	10.5

$$\sigma = V_1 \sigma_{6063} + V_2 \sigma_{Al-(TiB_2+TiC)} \quad (1)$$

where σ_{6063} and $\sigma_{Al-(TiB_2+TiC)}$ are UTS of original 6063 and Al-(TiB₂+TiC)_p sheets, respectively. V_1 and V_2 are the corresponding volume fractions, which are 0.54 and 0.46 in the composite after one cycle. σ is calculated to be 167.9 MPa. Therefore.

UTS of the composite after the first cycle is much higher than that calculated one, indicating that the efficient strengthening of the laminated structure for the composite materials during the ARB process. Furthermore, both the tensile strength and ductility of the laminated composites are increased with increasing ARB cycles. Fig. 8b shows the variation of UTS, YS and EL of the composites with increasing ARB cycles, which are enhanced simultaneously. After three cycles, values of UTS, YS and EL increase to ~255.8 MPa, 247.4 MPa and 11.6%, increased by 21.9%, 22.4% and 17.2% compared with those after one cycle, respectively. Therefore, the good comprehensive mechanical properties demonstrate significant

superiority of heterogeneous laminated structure in mechanical enhancement.

In order to analyze the enhanced tensile mechanical properties of the laminated composites with increasing ARB cycles, the strain hardening behaviors of these composites are compared in Fig. 9. It shows that the uniform elongation of the laminated composites was increased continuously with increasing ARB cycles, as shown by the true stress and strain curves in Fig. 9a. The strain hardening rate (Θ) is calculated according to the formula:

$$\Theta = \frac{\partial \sigma}{\partial \epsilon} \quad (2)$$

where σ is the true stress and ϵ is the true strain. The truncation of true stress-strain curves and strain hardening rate curves relies on Considère criterion [24]:

$$\sigma = \left(\frac{\partial \sigma}{\partial \epsilon} \right)_{\epsilon} \quad (3)$$

As illustrated in Fig. 9b, the value of Θ decreased rapidly with increasing strain. But the values of the 2c and 3c samples are much higher than that of 1c sample, when the strain is smaller than ~2.35% as indicated by the red arrow. At a higher strain, Θ value of 2c sample drops rapidly and becomes lower than that of 1c sample. While, 3c sample always has the best Θ -retention and the highest strain hardening rate throughout the entire tensile deformation. It demonstrates that the strain hardening rate of the laminated composites was enhanced with increasing ARB cycles, which lead

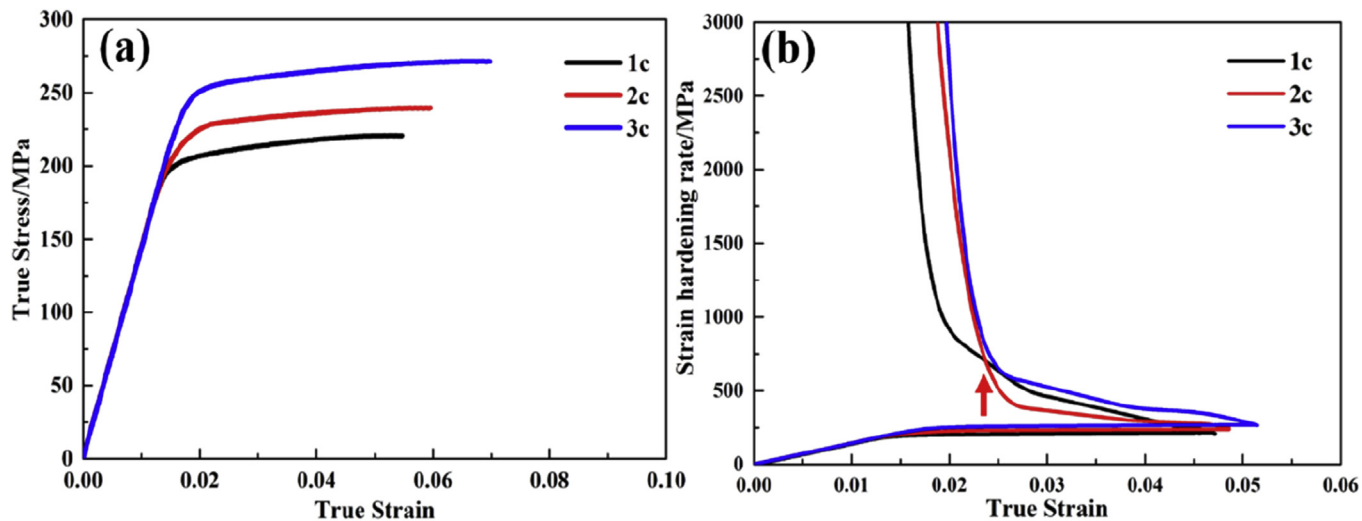


Fig. 9. (a) true stress–strain curves of the different composites; (b) the corresponding strain hardening rate curves of the three samples.

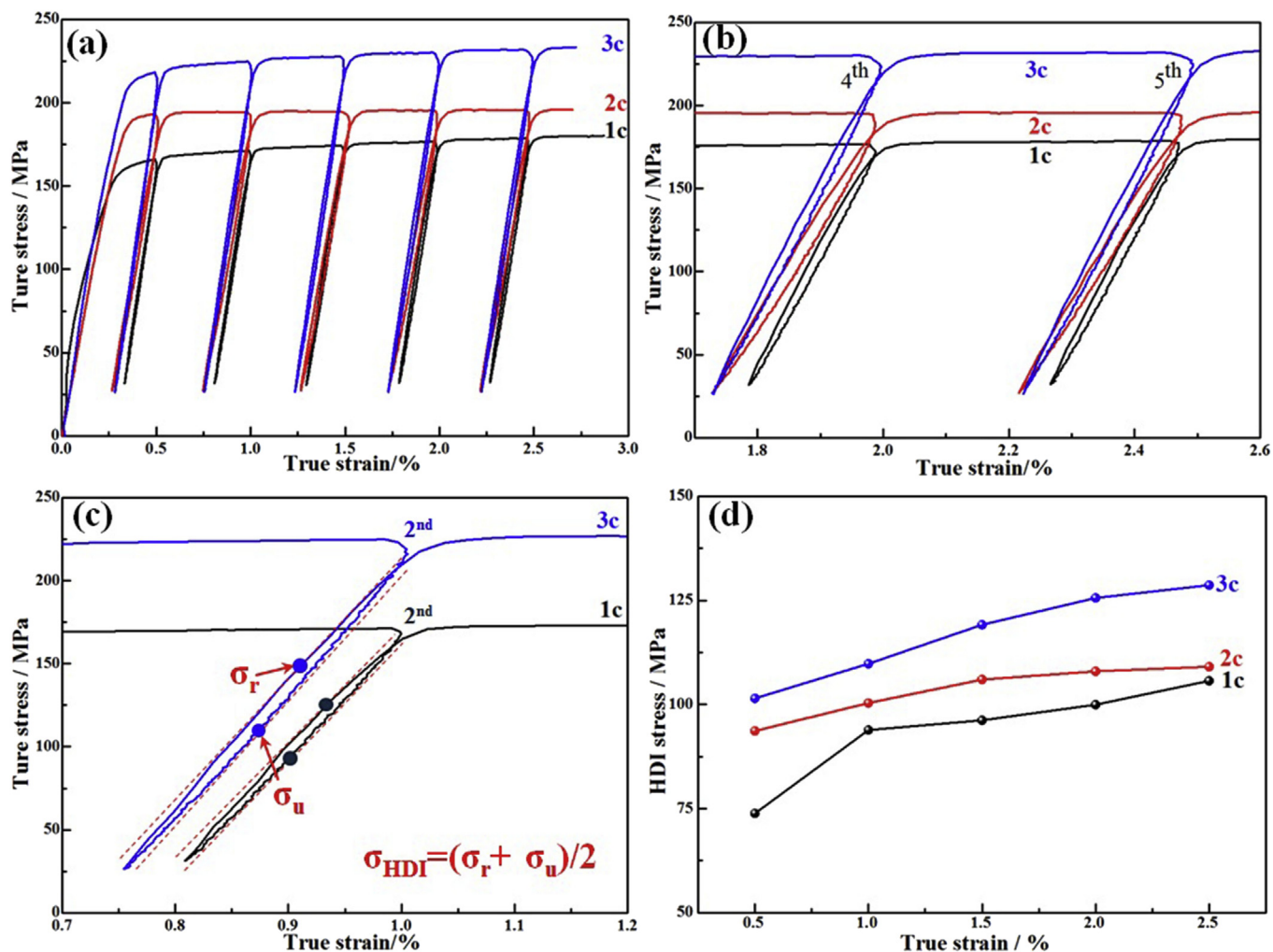


Fig. 10. HDI stress of Al-(TiB₂+TiC)_p/6063 composites with different cycles: (a) LUR stress–strain curves; (b) hysteresis loops of the 4th and 5th cycles; (c) the 2nd measured hysteresis loop with σ_u and σ_r defined; (d) HDI stress of the three samples versus applied strain.

to the increased ductility of the composites.

3.3. HDI stress strengthening in laminated Al-(TiB₂+TiC)_p/6063 composites

The main reason for the increased strain hardening (Fig. 9) can be attributed to the lamellar structure and the increased heterogeneous interfaces in the composites [25,26]. It has been reported that the elongated grains produce higher strain hardening than spherical ones, especially when its long axis is aligned in the loading directions. The lamella geometry makes mutual constraint between the soft and hard lamellae more effective, which produce higher HDI hardening. Besides, dislocations can pile up at the interlamella interfaces and accumulate to enhance the HDI hardening.

To probe the high strain hardening and the contribution of HDI stress to the observed yield strength, we conducted Loading-Unloading-Reloading (LUR) testing to estimate the contributions of the HDI hardening to the flow stress. Fig. 10a shows the LUR test hysteresis loops measured at varying tensile strains for three ARB treated composites. The HDI stress (σ_{HDI}) at different tensile strains can be calculated by the following equation (1) [26]:

$$\sigma_{\text{HDI}} = \frac{\sigma_r + \sigma_u}{2} \quad (4)$$

where the σ_r and σ_u is the reloading yield stress and unloading yield stress (as indicated in Fig. 10c). As shown in Fig. 10d, the HDI stress increased with the increasing strain, especially at the early stage, which contributed to the high strain hardening. HDI stress is about 128.7 MPa near the yield point with a strain of ~2.5% for the composites with three ARB cycles, which is ~56.7% of the flow stress. It also increases significantly with increased ARB cycles, which is mainly due to the increased lamellar interfaces at higher cycles. With increasing cycles, the number of interlamella interfaces between hard domains and soft domains per unit area is increased. GNDs will be generated to accommodate the strain gradient [27], leading to the development of high HDI stress [4,25]. Therefore, it is revealed that the high HDI stress contributes significantly to the enhanced strength of the laminated composites.

In addition to the high HDI hardening in the laminated composites, other strengthening mechanism including grain boundaries strengthening, dislocation strengthening, precipitation strengthening and the strengthening induced by the reinforcement particles, are also responsible for the enhanced tensile strength during ARB treatment. Revealing the HDI hardening in the heterogeneous laminated structured composites will supply the scientific guidance for the design and fabrication of high performance structure materials.

4. Conclusions

- (1) Laminated Al-(TiB₂+TiC)_p/6063 composites were successfully fabricated by ARB process up to three cycles. The laminated interfaces were well bonded and kept straight without any necking or fracture throughout the entire plastic deformation process. Meanwhile, TiC and TiB₂ particle became more dispersive during the deformation process, in addition to significant grain refinement of the Al matrix.
- (2) The tensile strength and ductility of the laminated composites were increased simultaneously with increasing ARB cycles. Compared with the composite after one cycle, UTS, YS and EL increase to 255.8 MPa, 247.4 MPa and 11.6% after three ARB cycles, increased by 21.9%, 22.4% and 17.2%, respectively.

- (3) It shows that the strain hardening rate of the laminated composites was enhanced with increasing ARB cycles, which lead to the increased ductility of the composites. Hetero-deformation induced (HDI) stress developed by GNDs at the heterogeneous interface, contributes significantly to the enhanced strength, which reaches up to ~56.7% of the flow stress near the yield point.

Acknowledgements

This work is supported by the National Key R&D Program of China (No. 2017YFA0204403) and the Natural Science Foundation of China (Nos. 51731007 and 51501092 and 2012CB932203). The authors also want to acknowledge the support of the Jiangsu Key Laboratory of Advanced Micro-Nano Materials and Technology. SEM, TEM and EBSD experiments are performed at the Materials Characterization and Research Center of Nanjing University of Science and Technology.

Appendix A. Supplementary data

Supplementary data to this article can be found online at <https://doi.org/10.1016/j.jallcom.2019.152285>.

References

- [1] X.B. Zhang, Y.B. Yu, B. Liu, J.Q. Ren, Mechanical properties and tensile fracture mechanism investigation of Al/Cu/Ti/Cu/Al laminated composites fabricated by rolling, *J. Alloy. Comp.* 805 (2019) 338–345.
- [2] J.F. Nie, M.X. Liu, F. Wang, Y.H. Zhao, Y.S. Li, Y. Cao, Y.T. Zhu, Fabrication of Al/Mg/Al composites via accumulative roll bonding and their mechanical properties, *Materials* 9 (2016) 951.
- [3] L.L. Meng, X.J. Wang, X.S. Hu, H.L. Shi, K. Wu, Role of structural parameters on strength-ductility combination of laminated carbon nanotubes/copper composites, *Compos. Part A* 116 (2019) 138–146.
- [4] Y.T. Zhu, X.L. Wu, Perspective on hetero-deformation induced (HDI) hardening and back stress, *Mater Res Lett* 7 (2019) 393–398.
- [5] X.L. Wu, M.X. Yang, F.P. Yuan, G.L. Wu, Y.J. Wei, X.X. Huang, Y.T. Zhu, Heterogeneous lamella structure unites ultrafine-grain strength with coarse grain ductility, *Proc. Natl. Acad. Sci. U.S.A.* 112 (2015) 14501–14505.
- [6] X.L. Wu, Y.T. Zhu, Heterogeneous materials: a new class of materials with unprecedented mechanical properties, *Mater Res Lett* 5 (2017) 527–532.
- [7] M.Z. Qadir, O. Al-Buhamad, L. Bassman, M. Ferry, Development of a recovered/recrystallized multilayered microstructure in Al alloys by accumulative roll bonding, *Acta Mater.* 55 (2007) 5438–5448.
- [8] N. Tsuji, Y. Ito, Y. Saito, Y. Minamino, Strength and ductility of ultrafine grained aluminum and iron produced by ARB and annealing, *Scr. Mater.* 47 (2002) 893–899.
- [9] L. Ghalandari, M.M. Mahdavian, M. Reihanian, Microstructure evolution and mechanical properties of Cu/Zn multilayer processed by accumulative roll bonding (ARB), *Mater. Sci. Eng. A* 593 (2014) 145–152.
- [10] Y.J. Zhang, N.H. Ma, H.W. Wang, Y.K. Le, X.F. Li, Damping capacity of in situ TiB₂ particulates reinforced aluminum composites with Ti addition, *Mater. Des.* 28 (2007) 628–632.
- [11] I.S. Lee, C.J. Hsu, C.F. Chen, N.J. Ho, P.W. Kao, Particle-reinforced aluminum matrix composites produced from powder mixtures via friction stir processing, *Compos. Sci. Technol.* 71 (2011) 693–698.
- [12] E. Ghasali, A. Pakseresht, F. Safari-Kooshali, M. Agheli, T. Ebadzadeh, Investigation on microstructure and mechanical behavior of Al-ZrB₂ composite prepared by microwave and spark plasma sintering, *Mater. Sci. Eng. A* 627 (2015) 27–30.
- [13] J.F. Nie, F. Wang, Y.S. Li, Y.F. Liu, X.F. Liu, Y.H. Zhao, Microstructure and mechanical properties of Al-TiB₂/TiC in situ composites improved via hot rolling, *Trans. Nonferrous Metals Soc. China* 27 (2017) 2548–2554.
- [14] Y.F. Liu, F. Wang, Y. Cao, J.F. Nie, H. Zhou, H.B. Yang, X.F. Liu, X.H. An, X.Z. Liao, Y.H. Zhao, Y.T. Zhu, Unique defect evolution during the plastic deformation of a metal matrix composite, *Scr. Mater.* 162 (2019) 316–320.
- [15] J.F. Nie, F. Wang, Y.S. Li, Y. Cao, X.F. Liu, Y.H. Zhao, Y.T. Zhu, Microstructure evolution and mechanical properties of Al-TiB₂/TiC in situ aluminum-based composites during accumulative roll bonding (ARB) process, *Materials* 10 (2017) 109.
- [16] A. Hanna, H. Azzeddine, R. Lachhab, T. Baudin, A. Helbert, F. Brisset, Y. Huang, D. Bradai, T.G. Langdon, Evaluating the textural and mechanical properties of an Mg-Dy alloy processed by high-pressure torsion, *J. Alloy. Comp.* 778 (2019) 61–71.
- [17] M. Alizadeh, M. Samiei, Fabrication of nanostructured Al/Cu/Mn metallic multilayer composites by accumulative roll bonding process and investigation

- of their mechanical properties, *Mater. Des.* 56 (2014) 680–684.
- [18] G. Min, J.M. Lee, S.B. Kang, H.W. Kim, Evolution of microstructure for multilayered Al/Ni composites by accumulative roll bonding process, *Mater. Lett.* 60 (2006) 3255–3259.
- [19] L. Su, C. Lu, A.K. Tieu, G.Y. Deng, X.D. Sun, Ultrafine grained AA1050/AA6061 composite produced by accumulative roll bonding, *Mater. Sci. Eng. A* 559 (2013) 345–351.
- [20] M. Alizadeh, M.H. Paydar, Fabrication of nanostructure Al/SiC_p composite by accumulative roll-bonding (ARB) process, *J. Alloy. Comp.* 492 (2010) 231–235.
- [21] F. Kümmel, M. Kreuz, T. Hausöl, H.W. Höppel, M. Göken, Microstructure and mechanical properties of accumulative roll-bonded aa1050a/AA5005 laminated metal composites, *Metals* 6 (2016) 56.
- [22] E. Bagherpour, M. Reihanian, H. Miyamoto, Tailoring particle distribution non-uniformity and grain refinement in nanostructured metal matrix composites fabricated by severe plastic deformation (SPD): a correlation with flow stress, *J. Mater. Sci.* 52 (2017) 3436–3446.
- [23] J.M. Lee, B.R. Lee, S.B. Kan, Control of layer continuity in metallic multilayers produced by deformation synthesis method, *Mater. Sci. Eng. A* 406 (2005) 95–101.
- [24] M.X. Yang, D.S. Yan, F.P. Yuan, P. Jiang, E. Ma, X.L. Wu, Dynamically reinforced heterogeneous grain structure prolongs ductility in a medium-entropy alloy with gigapascal yield strength, *Proc. Natl. Acad. Sci. U.S.A.* 115 (2018) 7224–7229.
- [25] X.L. Wu, P. Jiang, L. Chen, F.P. Yuan, Y.T. Zhu, Extraordinary strain hardening by gradient structure, *Proc. Natl. Acad. Sci. U.S.A.* 111 (2014) 7197–7201.
- [26] M.X. Yang, Y. Pan, F.P. Yuan, Y.T. Zhu, X.L. Wu, Back stress strengthening and strain hardening in gradient structure, *Mater. Res. Lett.* 4 (2016) 145–151.
- [27] H.J. Gao, Y.G. Huang, Geometrically necessary dislocation and size-dependent plasticity, *Scr. Mater.* 48 (2003) 113–118.